Femtosecond real-time probing of reactions. V. The reaction of IHgI

M. Dantus, R. M. Bowman, M. Gruebele, and A. H. Zewail
Arthur Amos Noyes Laboratory of Chemical Physics,[a] *California Institute of Technology, Pasadena, California 91125*

(Received 30 June 1989; accepted 15 August 1989)

The dissociation reaction of HgI_2 is examined experimentally using femtosecond transition-state spectroscopy (FTS). The reaction involves symmetric and antisymmetric coordinates and the transition-state is well-defined: $IHgI^* \rightarrow [IHgI]^{\ddagger *}_{Q_s \cdot Q_a \cdot q} \rightarrow HgI + I$. FTS is developed for this class of ABA-type reactions and recurrences are observed for the vibrating fragments (symmetric coordinate) along the reaction coordinate (antisymmetric coordinate). The translational motion is also observed as a "delay time" of the free fragments. Analysis of our FTS results indicates that the reaction wave packet proceeds through two pathways, yielding either $I(^2P_{3/2})$ or $I^*(^2P_{1/2})$ as one of the final products. Dissociation into these two pathways leads to HgI fragments with different vibrational energy, resulting in distinct trajectories. Hence, oscillatory behaviors of different periods in the FTS transients are observed depending on the channel probed ($\sim$300 fs to $\sim$1 ps). These results are analyzed using the standard FTS description, and by classical trajectory calculations performed on model potentials which include the two degrees of freedom of the reaction. Quantum calculations of the expected fluorescence of the fragment are also performed and are in excellent agreement with experiments.

I. INTRODUCTION

Femtosecond transition-state spectroscopy (FTS)[1,2] has been applied in this series of papers[3-6] to a number of chemical reactions of the type

$$AB^* \rightarrow [AB]^{\ddagger *} \rightarrow A + B \qquad (1)$$

as in the reactions of alkali metal halides[6,7] and

$$ABC^* \rightarrow [ABC]^{\ddagger *} \rightarrow AB + C \qquad (2)$$

as in the reaction of ICN.[3,4] More recently we have reported femtochemistry studies of the reaction of IHgI[8] (i.e., ABA), where the motion along two coordinates was observed. In this paper (V) new FTS results are presented for this reaction, and comparison with theory is made. These studies of the femtosecond dynamics in ABA-type reactions help us develop FTS in systems with more than one nuclear coordinate.

The HgI_2 system is attractive for several reasons. Firstly, it is much different from the case of ICN.[3,4] For ICN, the motion between the carbon and nitrogen atoms is considered frozen, allowing one to treat the ICN as a quasidiatomic. In the case of HgI_2, motion is expected between both iodine atoms and the mercury atom adding an additional coordinate on the potential energy surface (PES). Secondly, the equivalence of the two bonds make the PES symmetric with respect to the I, HgI coordinate and the reaction path is well defined along the antisymmetric coordinate (see Fig. 1). Thirdly, because of the change in the structure in going from the transition-state to the final products, one expects changes in vibrational excitation of HgI fragments produced from different starting conditions. Detection of the laser-induced fluorescence (LIF) at different wavelengths gives us a handle on the different vibrational states produced in the reaction. Fourthly, the bending motion leads to rotational excitation in the final products and this can be probed in real time, as reported recently.[8(b)] Finally, a great deal of information is available on the spectroscopy,[9] product-state distributions,[10(a)] and the half-[10,11] and full-collision ($Hg + I_2 \leftrightarrow HgI + I$)[12] dynamics. Molecular beam studies by the group of Bernstein[12] and theoretical calculations by Mayer *et al.*,[12] have provided the foundation for describing the PES of the ground state.

The dissociation of HgI_2 has been studied[9,10] and several observations have been made. Excitation at 310 nm most

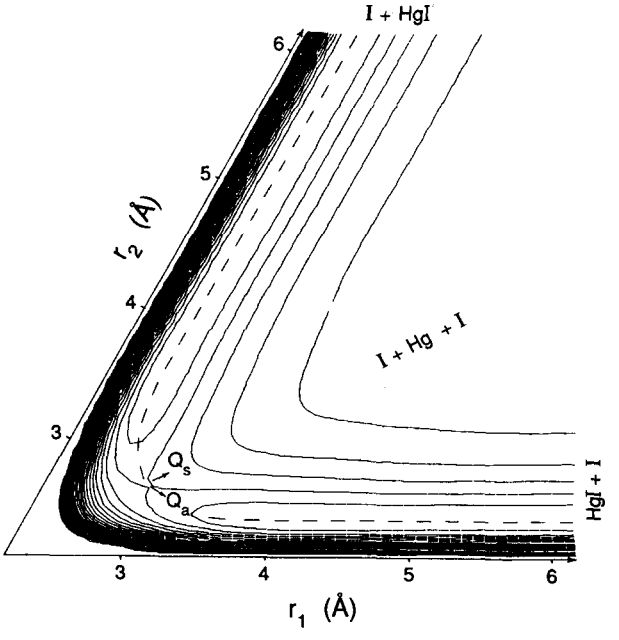

FIG. 1. Schematic of the mass-weighted PES for the reaction of linear HgI_2. The direction for the symmetric (Q_s) and antisymmetric (Q_a) stretches are indicated with arrows.

[a] Contribution No. 7971.

importantly accesses three dissociative channels of HgI_2[10]:

$$HgI_2 + h\nu \rightarrow HgI(X^2\Sigma) + I(^2P_{3/2}), \quad (3a)$$

$$\rightarrow HgI(X^2\Sigma) + I^*(^2P_{1/2}), \quad (3b)$$

$$\rightarrow Hg + I + I, \quad (3c)$$

producing iodine atoms in either the ground spin–orbit state $I(^2P_{3/2})$ or in the excited state $I^*(^2P_{1/2})$. At this wavelength of excitation it is known that the channel leading to ground state iodine [Eq. 3(a)] is preferred over the I^* channel [Eq. 3(b)] by about a factor of 4.[10(a)] The HgI fragment from both channels is produced in the ground electronic state ($X^2\Sigma$). FTS studies reported here are based on probing the HgI fragment during the dissociation and taking it to a second PES leading to the production of fluorescent HgI ($B^2\Sigma$). Due to the large change in the bond lengths from HgI ($X^2\Sigma$) to the excited state HgI ($B^2\Sigma$) the absorption and fluorescence spectra are very dispersed. Fortunately the spectroscopy has been analyzed by Cool *et al.*,[10(b)] and the Franck–Condon factors and assignments of these spectra are known.

The FTS analysis follows the guidelines described in the first paper of the series[3]; the new feature is the analysis of the fluorescence following the probing the transition states. Typically, the FTS signal involves the detection of the LIF generated by the probe laser. Probing of the reaction in real time can be achieved by tuning λ_2 (the probe laser) to a transition of the free fragment (λ_2^{∞} detection) or when it is tuned to transitions originating from transition configurations (λ_2^* detection). The fluorescence spectrum of HgI ($B^2\Sigma$), being well known, provides a unique opportunity for deducing which vibrational levels of the ground state HgI are accessed by the dissociation and which ones are accessed by the probe. Fixing the probe wavelength λ_2^*, and subsequently detecting the LIF at different wavelengths in a sense gives us the opportunity of discriminating the dynamics to a restricted set of trajectories. This new feature is exploited in this paper in order to map the PES for the HgI_2 dissociation reaction by the analysis of different trajectories observed in real time.

The organization of the paper is as follows: In Sec. II, we describe the experimental details specific to the FTS of HgI_2. This includes a discussion of a number of characterization and diagnostic experiments that we have performed. In Sec. III, we summarize the results. In Sec. IV the results are first discussed in terms of the simple FTS picture and then a comparison is made with classical two-dimensional trajectory calculations. Finally, a quantum mechanical analysis of the HgI fluorescence is performed and is used to deduce the experimental observations.

II. EXPERIMENTAL

The experimental methodology of FTS has been described in other femtochemistry studies.[3,4] In this section, we provide specific details pertinent to the FTS experiments of the HgI_2 reaction.

A. FTS experiments

Briefly, the femtosecond pulses were generated from a colliding pulse mode-locked ring dye laser (CPM),[13] and were amplified by a Nd:YAG-pumped pulsed dye amplifier (PDA).[14] The output pulses, as short as 50 fs duration, had 0.3–0.5 mJ of energy and 20 Hz repetition rate.

The pump wavelength (310 nm) was the second harmonic of the PDA output. Second harmonic generation was achieved in a thin (0.5 mm) KD*P phase-matched crystal. Two probe wavelengths were used in this studies. The output of the PDA at 620 nm was used without further conversion as a probe wavelength for experiments requiring tuning far off resonance of the free fragment transition. The probe pulses closer to the resonance transitions of the HgI ($X \leftrightarrow B$) states were generated by mixing the remainder of the PDA output with 1.06 μm light from the Nd:YAG laser in a thin (0.5 mm) KD*P crystal resulting in light at 390 nm. For experiments with 620 nm probing the pulses were as short as 50 fs, for $\lambda_1 = 310$ nm and $\lambda_2 = 390$ nm experiments we recorded cross correlations of 80 to 90 fs. In all cases care were exercised to insure that the pulses were chirp free (transform limited), so that $\Delta\nu\Delta t = 0.3$ to 0.5.

The pump and probe beams, with proper attenuation and parallel or perpendicular polarization, were delayed in time relative to one another in a Michelson interferometer, and were collinearly recombined and focused into the reaction chamber. Two custom made cells were used in these experiments. The first cell allows controlled flow of the HgI_2 and can be fitted with an electrode which we have used for determination of the absolute zero of time *in situ* by the DEA/MPI technique.[3,4] The second cell is a small quartz cylinder in which a small amount of HgI_2 is sealed in vacuum. Due to the fast recombination of I and HgI[9(a)] in the cell we confirmed that vapor flow was not necessary for our experiments. The static cell was used in most of the experiments because of its convenience.

LIF of the HgI fragment was collected at right angles to the direction of the pump/probe pulses through a $f/1.5$ lens arrangement. Spurious light and scattered light were rejected by dispersing the LIF through a 0.34 m monochromator. The LIF was collected at right angles by a photomultiplier tube (PMT), and a boxcar integrator averaged a portion of the PMT voltage. The entire experiment was controlled by a microprocessor, which adjusted the optical delay line of the Michelson interferometer and acquired and numerically averaged the boxcar output. Dispersed LIF spectra were acquired by a computer driven monochromator with the probe at a fixed delay with respect to the pump pulses. The fluorescence spectra were not corrected for laser intensity or PMT spectral response.

Characterization of the pump and probe pulses was performed for each data set. The characterization consisted of taking the spectrum of each of the pulses and measuring the time duration of the pulses. For $\lambda_1 = 310$ nm, $\lambda_2 = 390$ nm experiments,an autocorrelation of the PDA output in a noncollinear autocorrelator determined the temporal characteristics of the pulses. For 310/390 experiments a cross correlation technique using difference frequency generation in a nonlinear crystal ($\omega_{DFG} = \omega_{pump} - \omega_{probe}$) was used, the

light near 1.45 μm was detected with a germanium photodiode. The overall temporal response function of the apparatus was determined using the DEA/MPI technique.

B. Diagnostic experiments

The characterization of the HgI_2 reaction signal involved numerous diagnostic experiments. First, to establish the linearity of the signal with respect to the intensity of both the pump and the probe laser beams, the dependence of the LIF signal on the pump or probe energy was recorded. This measurement was made for transients resulting from $\lambda_1 = 310$ nm and $\lambda_2 = 390$ nm or 620 nm. The results are plotted on a log–log scale in Fig. 2. For each case the data falls on a line with a slope near unity, which is evidence for the linearity of the FTS experiment as well as the detection apparatus. As a further test, FTS transients for both probe wavelengths were taken under high and low intensity of both pump and probe beams. We observed no evidence of saturation in any of these measurements. The signal level is consistent with previous FTS experiments carried out in this laboratory taking into account various factors such as cross sections of the transitions, detector sensitivity and quantum yields.

In order to insure that the signal is due to the HgI_2 monomer and not polymers, and to determine the extent of collisional quenching of the signal we performed an experiment that compares the signal intensity to the theoretically calculated number density at different temperatures. The results of this experiment are presented in Fig. 3. The signal was found to closely follow the number density curve. Plotting the number density vs the signal [Fig. 3(b)], gives a straight line with a slope of unity indicating that in the range of pressures and temperatures used for these experiments the signal was not affected by collision quenching and it did not depend on dimers or polymers. All the data reported here was acquired in conditions far from the extremes used for these diagnostic experiments.

The pump beam (310 nm) was found to produce some background HgI fluorescence. A pump intensity dependence experiment similar to the experiments used to determine the linearity of the signal was performed in order to determine the dependence of this background fluorescence observed due to the pump alone. The background fluorescence was found to closely follow a straight line with a slope of 2 on a log–log scale [see Fig. 2(c)]. We consider this evidence that the signal is due to a two photon absorption of ground state HgI_2 producing HgI in the $B^2\Sigma$ state. Two photon LIF had been previously reported for HgI_2 by other experimenters.[9,10] In all of the data reported here this back-

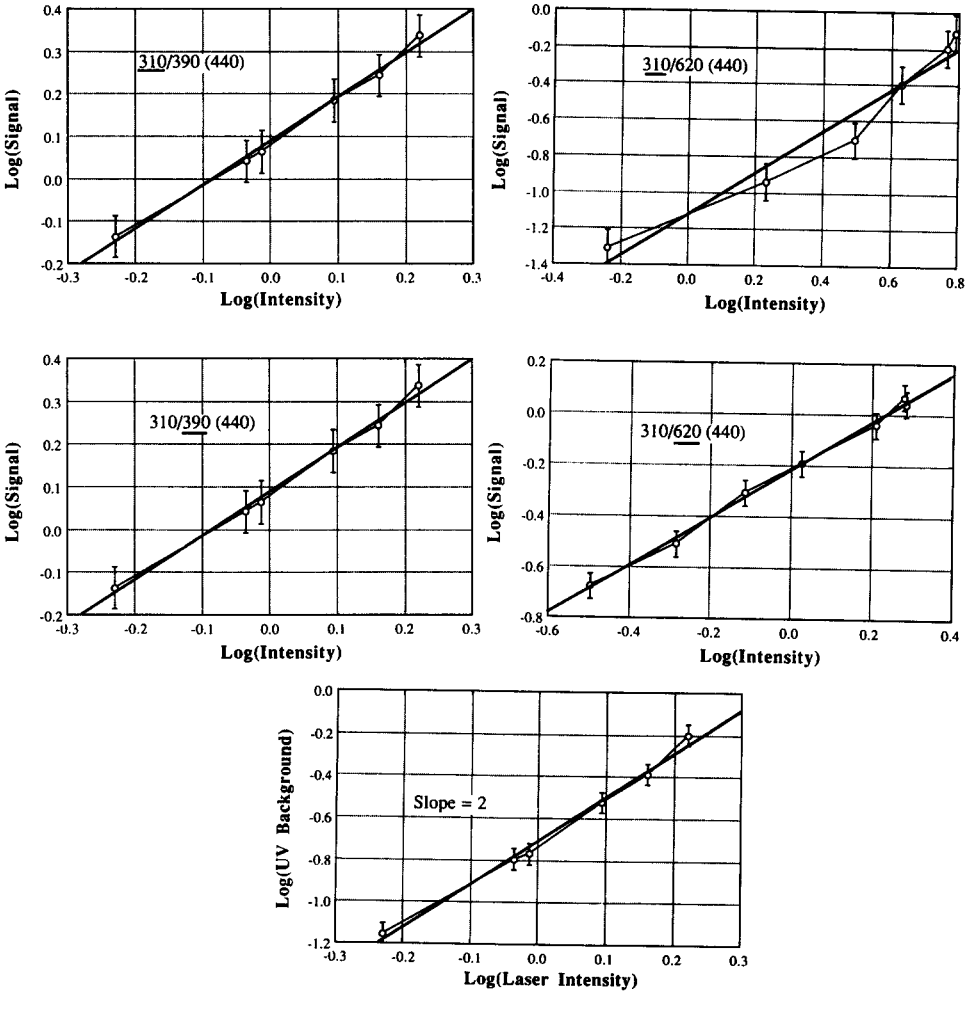

FIG. 2. Power dependence of the LIF signal. The observed LIF is plotted as a function of pump or probe (underlined) intensity on a log–log scale. (a) Pump and probe power dependences for $\lambda_1 = 310$ nm and $\lambda_2 = 390$ nm. (b) Pump and probe power dependences for $\lambda_1 = 310$ nm and $\lambda_2 = 620$ nm. (c) Pump alone, $\lambda_1 = 310$ nm, power dependence of LIF. The heavy lines shown are linear least squares best fits to the data. In (a) and (b) the slopes of the lines are near unity. In (c) the slope of the line is ~ 2.

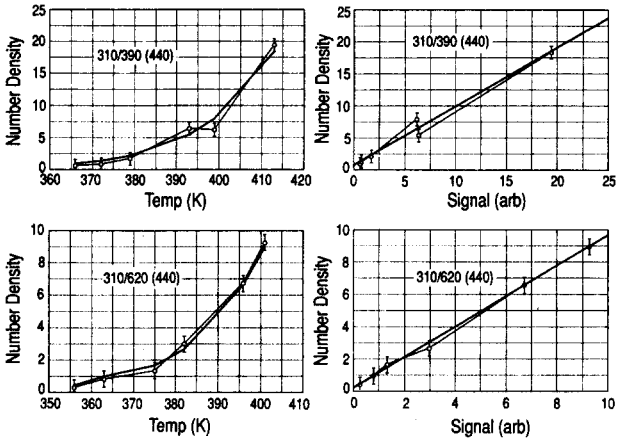

FIG. 3. LIF dependence on number density. The LIF signal and calculated number density are plotted vs temperature along with a plot of LIF signal versus number density. (a) Signals for $\lambda_1 = 310$ nm, $\lambda_2 = 390$ nm and $\lambda_1 = 310$ nm, $\lambda_2 = 620$ nm dependence on temperature (circles) and calculated number density dependence on temperature (heavy line). (b) Calculated number density vs detected signal (circles) for $\lambda_1 = 310$ nm, $\lambda_2 = 390$ nm and $\lambda_1 = 310$ nm, $\lambda_2 = 620$ nm. The heavy lines shown are linear least squares best fits to the data. The slopes are near unity.

ground was always kept to less than 10% of the total signal. The probe beam at 390 nm gave no such fluorescence background. The resulting LIF was dispersed in a monochromator and detection of the signal at wavelengths different than 390 nm assured no scattered light was collected. Probing with 620 nm light gave a very small amount of background fluorescence when allowed in the experimental cell with no attenuation. This background fluorescence was due to a multiphoton excitation. In all experiments this type of background fluorescence was kept to less than 1% of the total signal. It should be noted that the background level due to multiphoton fluorescence was time-delay independent and was easily reduced to a minimum by attenuation of the beams.

The absence of scattered light allowed us to position the gate of the boxcar integrator at time zero and to collect for approximately the width of two fluorescence lifetimes. Several gate widths and positions were tested. In all cases the FTS transient remained unaffected but signal levels and signal-to-noise ratios did change.

The polarization of the pump and probe beams were found to affect the transients but only in a manner predicted by alignment theory.[8(b),15] Good polarization extinction was insured for either parallel or perpendicular pump and probe beams before the nonlinear crystals and after the light had been converted. The effect of parallel vs perpendicular probing has been analyzed in detail.[8] All of the results presented here have been acquired with parallel polarization of both pump and probe beams except where specified.

Finally, the mercury(II) iodide used in this study (Aldrich) had a certified purity of 99.999% and was used directly without further purification. The sealed cell was extensively cleaned with dilute HF solution, rinsed thoroughly with distilled water and then flame cleaned before the introduction of the HgI_2. Following evacuation it was outgassed for several hours and then sealed. The *N,N*-diethylaniline (Aldrich, 98%) was fraction distilled until it became colorless and then was outgassed before every experiment.

III. RESULTS

As mentioned earlier, the HgI_2 reaction provides an extra degree of freedom, namely the participation of the two Hg–I bonds. The unbroken HgI bond may acquire substantial vibrational excitation which is manifested in the fluorescence spectra of the HgI product. Detection of the product LIF at different wavelengths is a new feature for FTS experiments and for its analysis we use a condensed notation. For the pump and probe wavelengths we use the conventional symbols λ_1 and λ_2, respectively. The detection wavelength we call λ_{det}. An experiment resulting from $\lambda_1 = 310$ nm, $\lambda_2 = 390$ nm, and $\lambda_{det} = 440$ nm will be described here as a 310/390 (440) experiment. Using this notation we present our results.

A. 310/390 results

As in an earlier communication,[8(a)] detection at 440 nm yielded the transient shown in Fig. 4(a). The signal consists of a very fast rise followed by a much slower decay to an asymptotic value of about 60% of the peak intensity. In addition to this behavior, oscillations are seen which last for many periods. The first period of 220 fs is different from the longer time oscillations which have a period of ~300 fs. Another transient reported previously was taken at 360 nm and is shown in Fig. 4(b). This transient also has a very fast rise, but then decays to a much smaller plateau value than

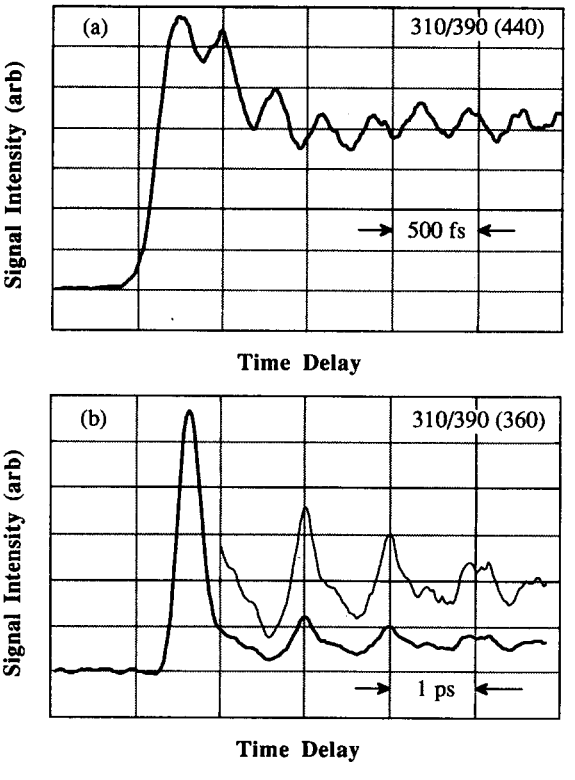

FIG. 4. Typical FTS transients for $\lambda_1 = 310$ nm and $\lambda_2 = 390$ nm. The detection wavelengths used are (a) $\lambda_{det} = 440$ nm and (b) $\lambda_{det} = 360$ nm. The thin line is $\times 3$ expansion of the transient. Note the differences in time scales.

the 440 nm transient, ~10% of the peak value. The oscillatory behavior at this wavelength is quite different than the 440 nm results. The difference between the first and second oscillation is 1.3 ps with the beam frequency then becoming regular at ~1 ps.

To identify the spectral changes we proceeded to disperse the fluorescence arising from the first peak of the transient (near time zero) and then we dispersed the fluorescence from the second oscillation 220 fs later. The two transient spectra are presented in Fig. 5 along with a difference spectrum. The spectrum taken at the first peak has a much broader feature at 440 nm than the more structured spectrum taken 220 fs later suggesting that the 310/390 (440) transient is a combination of (at least) two components. The largest difference between the transient spectra was found at 427.5 and 432.5 nm. Transients taken at these wavelengths are shown in Fig. 6. It should be noted that the slit width was narrowed to 0.5 mm at these wavelengths resulting in a monochromator bandwidth of 1.2 nm. This was as small a bandwidth as possible without cutting the signal-to-noise ratio to unacceptable values. Since these two wavelengths are only 5 nm apart, the narrow bandwidths minimized the spectral overlap of these transients. For all the other experiments mentioned in the results section the slit width had essentially no effect on the transient shape, so the experiments were run with slit widths of 2.0 mm (spectral resolution of 5.0 nm).

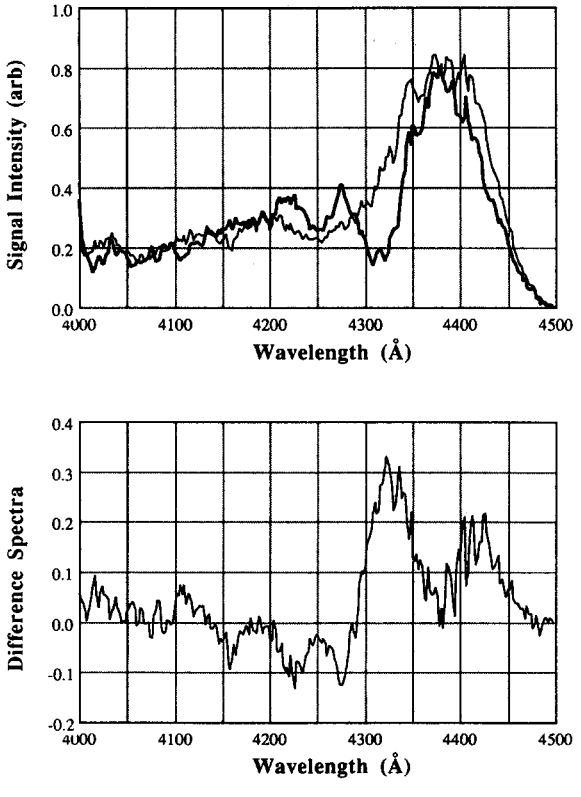

FIG. 5. (Top) Dispersed LIF spectra for $\lambda_1 = 310$ nm and $\lambda_2 = 390$ nm. The light line is for a delay time between pump and probe pulses corresponding to the first peak [in Fig. 4(a)]. The dark line is for a pump–probe delay corresponding to the second peak [in Fig. 4(a)]. (Bottom) The difference spectrum (light minus dark).

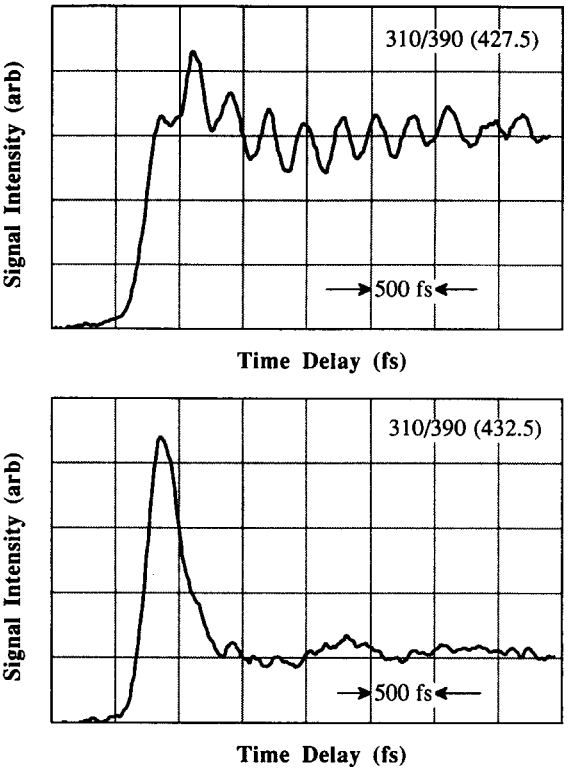

FIG. 6. FTS transients taken for $\lambda_1 = 310$ nm and $\lambda_2 = 390$ nm. The detection wavelengths used are (a) $\lambda_{det} = 427.5$ nm and (b) $\lambda_{det} = 432.5$ nm.

The transient taken at 427.5 nm is somewhat similar to the 440 nm transient described above. The major difference is the disappearance of the first oscillation. It now appears as a step instead of a peak. The oscillation frequency after the step is the ~300 fs, the same as reported for the 440 nm transient. In addition, the signal only decays to ~80% of the maximum value. The transient taken at 432.5 nm is almost identical to the 360 nm data. The only difference is the plateau level of around ~20% of peak value is slightly higher than for the 360 nm case. The oscillation pattern is the same, with the depth of modulation being similar.

Transients were recorded for every 5 nm interval from 350 to 450 nm. For all of the other wavelengths examined the behavior was similar to the behavior described above. For the detection wavelengths from 410 to 425 nm and longer than 435 nm the transients were almost identical to those reported at 440 nm. For wavelengths shorter than 370 nm the transients were very similar to the 360 nm transient. For wavelengths close to 390 nm there was a problem with scattered probe light, making it very difficult to record reliable transients.

B. 310/620 results

In this section results are given for $\lambda_1 = 310$ nm and for $\lambda_2 = 620$ nm. In the language of FTS, this corresponds to off-resonance probing, thus $\lambda_2 = \lambda_2^* = 620$ nm. Unlike the 310/390 nm data, the transients taken at these wavelengths all had the same general behavior. Shown in Fig. 7 are the results for three detection wavelengths: 440, 390, and 360 nm. Previously, the 440 nm and 390 nm data have been pub-

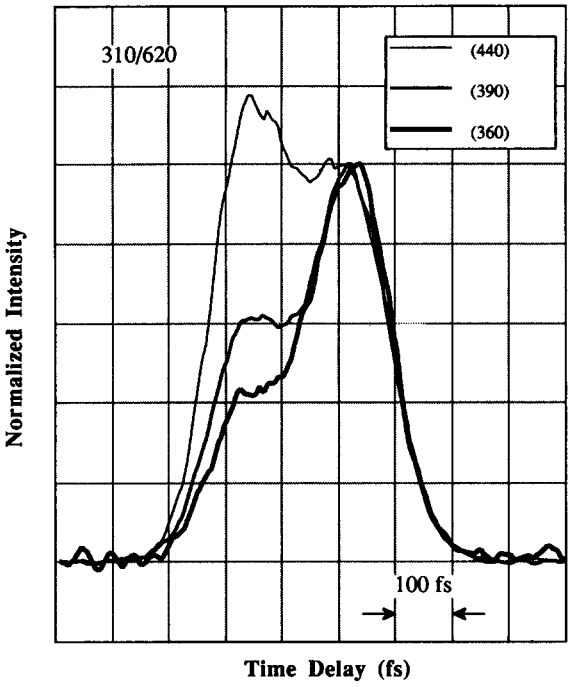

FIG. 7. FTS transients taken for $\lambda_1 = 310$ nm and $\lambda_2 = 620$ nm. The second peak intensity has been scaled to an intensity of 1.0 so comparisons can be made. The detection wavelengths for each transient are indicated in the legend.

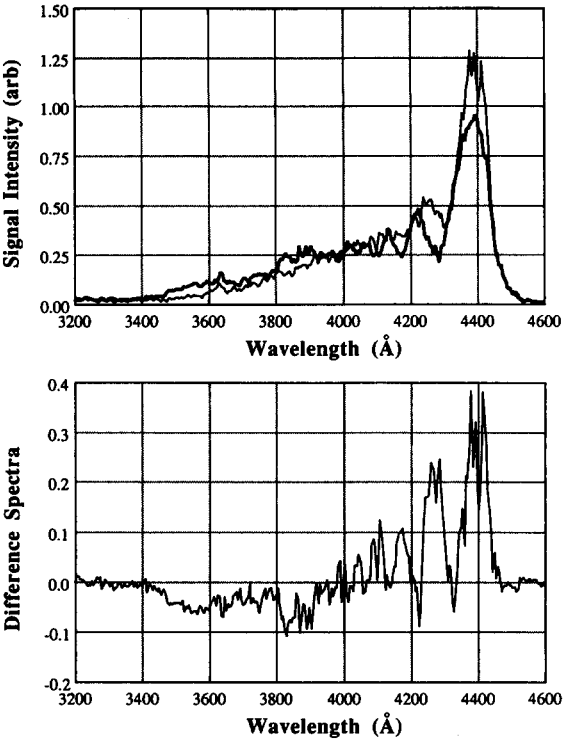

FIG. 8. (Top) Dispersed LIF spectra for $\lambda_1 = 310$ nm and $\lambda_2 = 620$ nm. The light line is for a delay time between pump and probe pulses corresponding to the first peak (in Fig. 7). The dark line is for the pump–probe delay corresponding to the second peak (in Fig. 7). (Bottom) The difference spectrum (light minus dark).

lished[8(a)] for perpendicular polarization of the pump and probe beams. All the transients consist of two peaks, i.e., a single oscillation. The only difference in these transients is the relative height of these peaks with respect to each other. Other features are an instrument response limited rise time and a decay to zero signal at times greater than 600 fs; this is a completely off-resonance transient. As the detection wavelength moves to the blue, the amplitude of the second peak grows with respect to the first peak (or the first peak amplitude decays with respect to the second).

Spectra were taken from 320 to 460 nm at probe time delays corresponding to the first peak and the second peak. These spectra are shown in Fig. 8. Again the spectra are very different. The spectra were subtracted and their difference spectrum is structured. Differences in the spectra will be discussed in the following sections.

IV. DISCUSSION

A. Preliminaries

The dissociation of HgI_2 occurs following excitation of the first long wavelength absorption band peaking at 265 nm and extending to 350 nm.[9,10] Quantum yield of iodine in both spin–orbit states has been determined by Leone's group.[10(a)] Production of $I^*(^2P_{1/2})$ was found to be favored for excitation at wavelengths shorter than 295 nm while at longer wavelengths the ratio of $I(^2P_{3/2})$ dominates. At 310 nm, the wavelength of interest for this study, one can estimate the production of $I^*(^2P_{1/2})$ to be $\sim 25\%$.[10(a)] Formation of the two spin–orbit states of iodine is believed to arise from separate potential energy surfaces of HgI_2.

The energetics of the reaction for HgI_2 vapor at 150 °C have been estimated as follows: Firstly, the thermal energy is estimated to be $5\ kT \approx 1500\ cm^{-1}$ (for rotation and vibration of a linear triatomic). Secondly, the dissociation energy for the reaction $HgI_2 \rightarrow$ ground state HgI and I is $\approx 21\,000\ cm^{-1}$ (the I–HgI is stable by -1.45 eV with respect to Hg and I_2 and the endoergicity of the reaction $Hg + I_2 \rightarrow HgI + I$ is 1.15 eV resulting in 2.6 eV for D_0 as determined by Wilcomb *et al.*[12]). Thirdly, the photon energy of the pump pulse at 310 nm is $32\,300\ cm^{-1}$, adding the thermal energy gives a total of $33\,800\ cm^{-1}$. Subtracting the dissociation energy from the total energy in the excited molecule yields $\sim 12\,800\ cm^{-1}$ of excess energy available for the recoil of the fragments and the vibration and rotation of the HgI fragment. If the rotational energy is $\approx 300\ cm^{-1}$ (assuming a Boltzmann distribution at 150 °C) it turns out that $12\,500\ cm^{-1}$ of energy is available for translation and vibration of the products. When the photodissociation involves the production of $I^*(^2P_{1/2})$ the spin–orbit coupling energy of $7600\ cm^{-1}$ must be subtracted leaving this channel with $4900\ cm^{-1}$ of available excess energy. Other useful constants are given in Table I, including the vibrational frequencies for HgI_2 and HgI.

In the following sections we discuss: the effect of FTS probing at different wavelengths, the discrimination of reaction trajectories accessed by different wavelength detection and how the FTS transient obtained are utilized to map the PES of the reaction.

B. FTS of the reaction

In light of past FTS studies on ICN[4] and alkali-halides[6,7] we first present an interpretation of the experiments

TABLE I. Spectroscopic constants for HgI_2 and HgI.

	HgI_2 (ground state)		ν_0 [a]	Period
Q_s	Symmetric stretch		155 cm^{-1}	215 fs
Q_a	Antisymmetric stretch		237 cm^{-1}	141 fs
q	Bend		33 cm^{-1}	1000 fs
D	Dissociation energy		21 000 cm^{-1}	
HgI ($X^2\Sigma$)[c]	ω_e [b]	125 cm^{-1}		period 267 fs
	D	2800 cm^{-1}	(dissociation energy)	
	β	7.09	($\beta^2 = \omega_e{}^2/4B_e$)	
	r_e	2.80 Å		
HgI ($B^2\Sigma$)[c]	ω_e [b]	110 cm^{-1}		period 303 fs
	D	18 850 cm^{-1}		
	β	2.86		
	r_e	3.30 Å		

HgI ($B \leftarrow X$) Transition dipole $\mu = 4 \exp[-(r-3.39)^2/0.9^2]$ Debye

[a] Values taken from Lowenschuss, Ron, and Schnepp, J. Chem. Phys. **50**, 2502 (1969).
[b] Values taken from Ref. 9(b).
[c] Values for D, β, and r_e have been chosen to give the best overall representation of the ground state potential energy function and the best representation of the accessed vibrational energy levels of the excited state.

treating the dissociation as occurring on a one-dimensional PES (see Fig. 9). The PES's drawn in Figs. 9 and 10 have been scaled with available spectroscopic[9-12] and thermodynamic[16] data and are helpful in presenting a first order understanding of the FTS transients obtained. The full two-dimensional interpretation of the results is left for the next section. Figure 9 shows the schematic for the pump–probe experiment. The pump pulse accesses both the I and I* PES (directly or indirectly through crossing) depositing a wave packet at time zero of the reaction. The probe wavelength, drawn to scale, interrogates the wave packets as they make their way to final products. In Fig. 10 we show all of the states accessible in our experiment, along with the HgI absorption shown on the left axis. Figure 11 is a schematic explaining how we detect different vibrational levels with fixed pump and probe wavelengths. Using the proper Franck–Condon factors and vibrational distributions (see the next section), we find that detection at 360 nm accesses high v'' in the HgI ground state and similarly detection at 427.5 nm accesses low v'' in that same state.

For all the experiments, the pump wavelength λ_1 was fixed at 310 nm while two probe wavelengths were used. The probe wavelength was either on resonance λ_2^{∞} for 390 nm or off-resonance λ_2^{*} for 620 nm (see Fig. 9). The distinction between on and off resonance is made here by the fact that for on-resonance probing, at 390 nm, the free HgI fragment absorbs the probe wavelength giving rise to an asymptotic

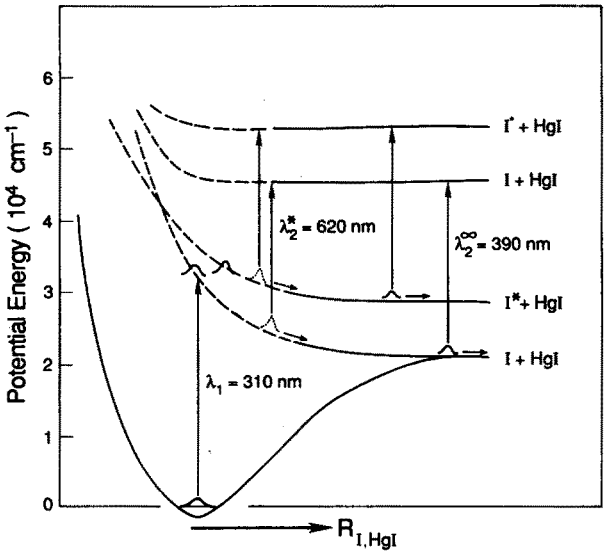

FIG. 9. Schematic of the FTS experiment with the pump and probe energies drawn to scale. At time zero the pump pulse deposits a wave packet in the I and I* channels. The probe pulses interrogate the motion of the wave packets at early times (620 nm) in the transition-state region or at later times (390 nm) as they become free fragments.

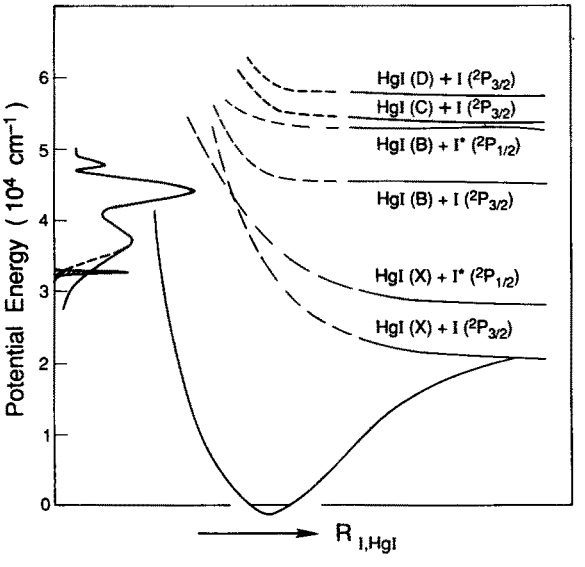

FIG. 10. Schematic of the one-dimensional PES of the HgI_2 dissociation. The absorption spectrum of HgI_2 [Ref. 10(a)] and the pump energy used are sketched on the left.

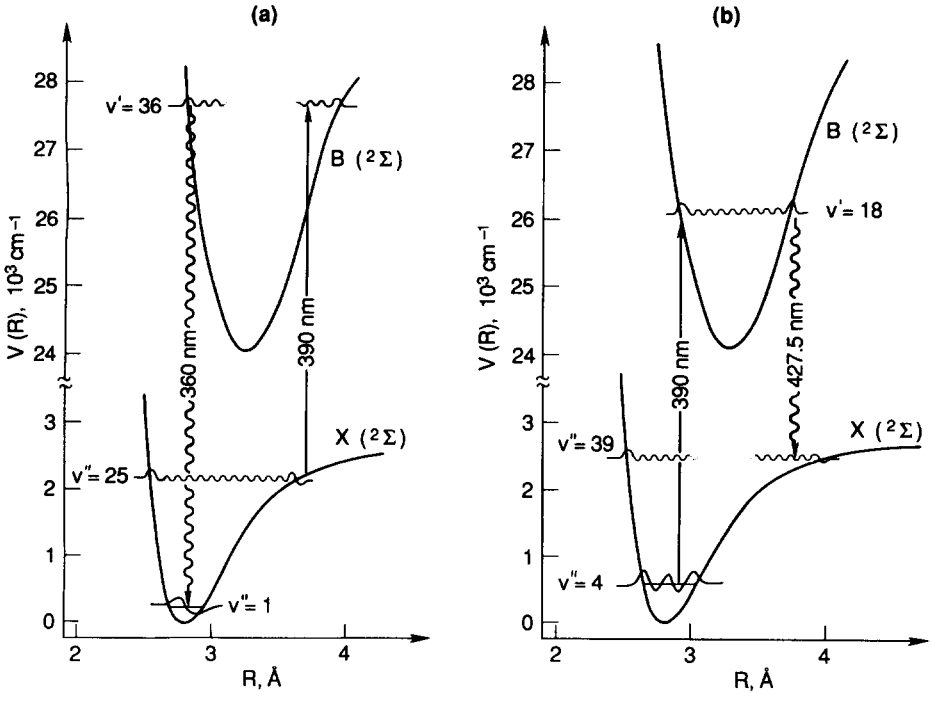

FIG. 11. Schematic of the HgI PES showing the effect of probing with 390 nm two vibrational distributions. (a) Probing a high vibrational level $v'' = 25$ leads to fluorescence at 360 nm. (b) Probing a low vibrational level $v'' = 4$ leads to fluorescence at 427.5 nm.

level in the transients where the coherent oscillations are present. In the off-resonance case, there is no transition of the free HgI which is resonant with the 620 nm probe. It is evident in the experimental transient that for 620 nm excitation the asymptote is at the same level as the base line, implying that there is no signal at longer times and that only fragments in the transition-state region absorb. Off-resonance signal is usually characterized by a rise from zero signal and decay to zero signal at short times. These rise and decay times can be related to the lifetime of the transition-state of the reaction for a given spectral window determined by the probe spectrum and convolved by the temporal duration of the pulses.[5]

Probing at $\lambda_2^{\infty} = 390$ nm we observe several types of transients which appear to be combinations of two distinct behaviors as seen in the data for 310/390(427.5) and 310/390(432.5). The transient obtained for 310/390(427.5) basically reaches a maximum and remains at the maximum level of signal for all times (neglecting the oscillations). The transient for 310/390(432.5) after the first peak near time zero shows the growth of an asymptotic level which shows long period oscillations lasting for long times.

For the analysis it is important to determine whether these two transients are spectrally pure. Subtracting 15% of the (427.5) transient from the (432.5) transient we obtain a transient that is very similar to the data taken at 360 nm [see Fig. 12(a)]. Thus, it appears that these transients are not entirely separated spectrally. Subtracting 67% of the (432.5) transient from the (427.5) data we obtain the tran-

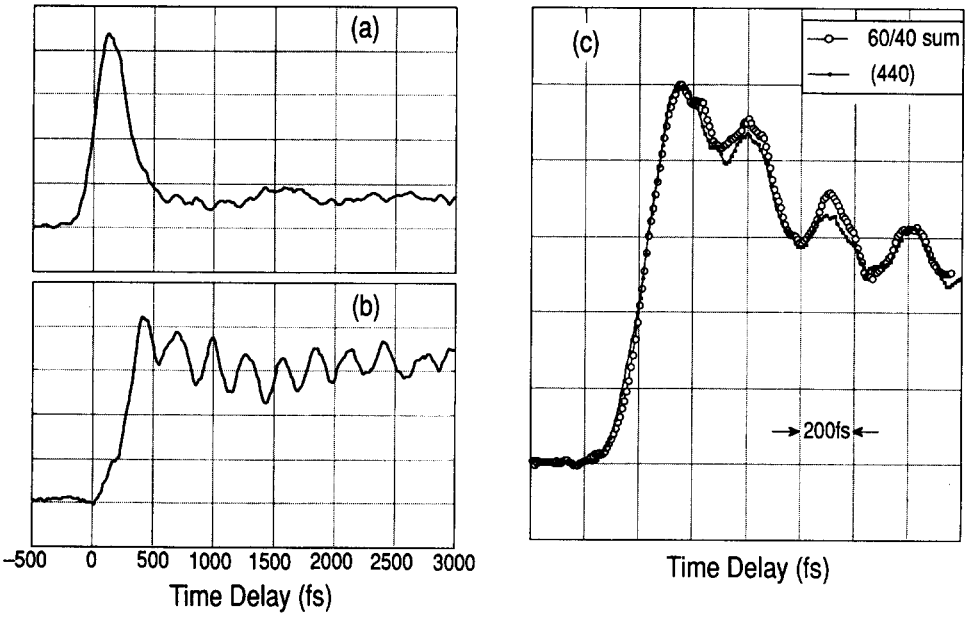

FIG. 12. (a) Transient resulting from subtracting 15% of the unnormalized 310/390 (427.5) transient (Fig. 6 top) from the unnormalized 310/390 (432.5) transient (Fig. 6 bottom). (b) Transient resulting from subtracting 67% of the unnormalized 310/390 (432.5) transient (Fig. 6 bottom) from the unnormalized 310/390 (427.5) transient (Fig. 6 top). Notice that ~300 fs delay between transient (a) and (b) indicating "on- and off-resonance-like" behavior. (c) Transient (circles) resulting from addition of 60% of the unnormalized 310/390 (427.5) transient with 40% of the unnormalized 310/390 (432.5) transient. The transient has been scaled to show the similarities with the 310/390 (440) transient published in Ref. 8(a) (black squares).

sient shown in Fig. 12(b). There is clearly a delay from time zero before the signal begins to rise (see below). So the data taken detecting at (427.5) and (432.5) are made up of the two pure transients shown in Figs. 12(a) and 12(b). As further proof in Fig. 12(c) we show that the previously published 310/390(440) transient can be understood as a combination of the (427.5) and (432.5) data. This is clear indication that all of the HgI_2 experiments performed at 310/390 give rise to two distinct behaviors: a transient similar to the 310/390(360) data and the transient shown in Fig. 12(b).

The analysis of these FTS on-resonance transients yields the "clocking" time of the reaction.[4] Briefly, the clocking experiment can be described as follows. During the dissociation the fragments are in the process of becoming free particles. The internuclear distance between the fragments determines the extent of the perturbation that one fragment has on the other. The clocking experiments determines at which point in time (and distance) the products are spectroscopically distinguishable as free particles. Fully on-resonance FTS transients have a delay time ($\tau_{1/2}$) that is associated with the time it takes the free fragment absorption to "turn on." This can be clearly seen in Fig. 12(b), where a $\tau_{1/2}$ of ~ 300 fs is found.

The transients obtained with $\lambda_2^{\infty} = 390$ nm can be understood in terms of two reaction channels producing two types of behaviors. As mentioned in the results section the period separation gives the vibrational energy content of the HgI fragment and we can therefore determine the amount of recoil energy. From the transient in Fig. 12(b) we consider the frequency of the oscillations (~ 300 fs) and we match it to the corresponding vibrational spacing of the HgI in the ground state (for this case $v'' = 7 \pm 1$). Using a similar calculation for the transient in Fig. 12(a) we obtain $v'' = 29 \pm 2$.

From these numbers it is possible to determine the amount of vibrational excitation in the dissociating fragments. Remembering, that energetically it is possible to produce iodine in its ground state ($^2P_{3/2}$) or the spin–orbit excited state ($^2P_{1/2}$), gives four possibilities for the total amount of energy for recoil [11 800 or 10 000 cm^{-1} for the I($^2P_{3/2}$) and 4200 or 2400 cm^{-1} for I*($^2P_{1/2}$)]. These energies can now be converted to the terminal velocity in the center of the mass of the fragments. For now, assume that the I channel leads to HgI with high vibrational excitation, i.e., 10 000 cm^{-1} are available for translation, while the I* channel leads to low vibrational excitation, i.e., 4200 cm^{-1} go into translation. Thus, the terminal velocity at which I recoils after dissociation is 1.6×10^{-2} Å/fs while the I* terminal velocity is calculated to be 1.0×10^{-2} Å/fs. Taking the I and I* PES to be simple one-dimensional exponentials with a typical length parameter ($L = 0.6$ Å), we can estimate the time of arrival of free HgI to be 220 and 300 fs for the I and I* channels,respectively. These calculations give a good estimate for the dissociation dynamics but the PES for both channels has been oversimplified and more accurate calculations require full consideration of other degrees of freedom as discussed later.

The (360) transients show a fast rise (that is very close to time zero) and then a fast decay. In addition, the asymptote level is a small percentage of the peak signal. There are two possible explanations for this large signal intensity at early times: the most favorable transition dipole moment is reached early in time near the transition-state region and/or the transition-state complex probed at early times undergoes complete dissociation to Hg + I + I. From the diagram in Fig. 10 it is clear that higher states are accessible with 390 nm probing at very short internuclear distances. We have recorded a transient detecting at 290 nm, probably due to fluorescence from the C or D states, which are accessed very near the time zero of the reaction by the 390 probe laser.

The off-resonance signals obtained with $\lambda_2^* = 620$ nm probe the transition-state region. At every detection wavelength the form of the transients is the same, consisting of two peaks separated by ~ 220 fs. The spectra taken at each of these peaks are different (see Fig. 8) indicating that these transients may come from two different channels (similar to the explanation for the 310/390 experiments). This is easily understood; since the channels have different energetics, the time it takes for each to arrive in the probing region could certainly be different (the time between the two peaks). If we consider that the two peaks are independent signals, then the width of the peaks can give an estimate of the life time of the transition-state accessed at this wavelength. This lifetime is on the order of 50 fs, implying that the probing is done on a steep (highly repulsive) part of the potential.

The interpretation of the HgI_2 transients we have obtained in terms of one-dimensional FTS theory is rather limited. In order to fully appreciate the molecular dynamics for this triatomic molecule one more coordinate is needed. It is the motion along the two Hg–I coordinates that determines the behavior of the transients. Classical, semiclassical, and quantum mechanical simulations have been performed (see below) in order to determine the trajectories responsible for the transients obtained experimentally. The results of these simulations and further refinement in our understanding of the reaction follows.

C. Two-dimensional FTS and the potential surface

We now turn to a more quantitative, yet still very simple analysis of the FTS experiments in terms of classical trajectories on a two-dimensional PES for the I–Hg–I system. In part 1, we review our choice of the PES, and the results of the trajectory calculations. In part 2, the quantum mechanical calculation of the HgI fluorescence and a semiquantitative comparison with the transients shown earlier will be presented.

1. PES and classical trajectory calculations

The potential energy function of HgI has been studied extensively by emission spectroscopy,[9(b),10(b)] and the asymptotic behavior of the full PES, insofar as it can be represented by Morse potentials, is well known. On the other hand, the nature of the $^1\Sigma_g^+$ HgI_2 surface giving rise to the HgI (X) + I and HgI(X) + I* channels accessed by the pump beam, and of the $^1\Sigma_u^+$ surface giving rise to the HgI(B) + I and HgI(B) + I* states accessed by the probe

beam, is largely unknown. Relativistic *ab initio* calculations on $HgCl_2$ by Wadt[17] indicate that these states will be bent by 80°–100°. However, the vertical pump transition from the ground state will most likely access the upper state in a linear configuration, given that the bending mode of HgI_2 is only thermally excited. Furthermore, the coupling of the bending motion with fragment rotation and translation occurs on a time scale of picoseconds and plays a lesser role in the bond breaking process near the transition state. The rotational dephasing of HgI_2 has been discussed in detail in Ref. 8(b); we will concentrate on a two-dimensional approach involving the asymmetric and symmetric stretching coordinates of HgI_2 and translation and stretching vibration of the fragment instead. We thus confine ourselves to an understanding of the motions within the first 1–2 ps, after which the breaking of the bond is complete, with the understanding that any PES described below represent appropriate rotational and bending vibrational averages.

Since reliable knowledge about the PES is limited, an empirical surface, such as a LEPS potential, must be used.[18] We have chosen a more flexible damped Morse surface, which can be used in quantitative fitting of the FTS spectra, when combined with a fully quantum mechanical treatment. Its general form is

$$V(r_1 r_2) = D\{1 - \exp\{-\beta [e^{-\gamma r_1}(r_1 - r_e)/r_e + e^{-\gamma r_2}(r_2 - r_e)/r_e]\}\}^2 - D, \quad (4)$$

where r_1 and r_2 are the two Hg–I bond lengths; D, β, and r_e are the dissociation energy, Morse coefficient, and equilibrium bond length along the reaction coordinate, and may depend on the deviation of the triatomic arrangement from a symmetric configuration; for the present purpose, they were represented as

$$f = f_0 + f_1 \exp[-(r_1 - r_2)^2/\sigma^2] \quad (5)$$

with $\beta_0 = 7.09, \beta_1 = 0.5, D_0 = 2800\,\mathrm{cm}^{-1}, D_1 = -1000\,\mathrm{cm}^{-1}, r_{e0} = 2.8$ Å, $r_{e1} = 0.4$ Å, $\sigma_{\beta,r} = 1.5$ Å and $\sigma_D = 1$ Å. This yields a good approximation to the potential function of HgI in the separated fragments limit, with a dissociation energy (in the symmetric stretch direction) of $1800\,\mathrm{cm}^{-1}$ at the saddle point, and a symmetric stretching frequency at the transition state slightly higher than the HgI stretching frequency. The tightness of the transition state is determined by β_1, which gives a very loose transition state when negative, and an increasingly tight transition state when positive. γ determines how fast the PES approaches an asymptotic I + HgI or IHg + I channel, and was chosen to be 1.5 Å. The resulting PES is shown in Fig. 13; with the above choice of parameters, the asymptotic region is well represented, and the transition region resembles a LEPS potential derived from the positive and negative contributions to the Morse potential of HgI. Of all PES tested, the above agreed best with the experimental measurements.

Before attempting a calculation, another simplifying assumption was made. Since the spin–orbit coupling is about $7600\,\mathrm{cm}^{-1}$, while the dissociation energy of HgI is only about $3000\,\mathrm{cm}^{-1}$, a crossing of the surfaces leading to the I and I* channels at internuclear separations larger than the ground state geometry is unlikely to yield the observed results, although it cannot be excluded as a possibility. Rather than postulating excitation by the pump beam to a single (I*) surface, followed by Landau–Zener crossing, we assume the picture of two nearly parallel surfaces leading to the I and I* channels, as shown schematically in Fig. 10. Furthermore, the two PES will be taken to differ only by the spin–orbit splitting in iodine, i.e., they are vertically shifted versions of the same functional form Eq. (4). That this assumption is reasonable can be seen if the I/I* branching ratio measured by Hofmann and Leone[10(b)] is interpreted in terms of two independent potential surfaces: I* formation is resonant at 265 nm, while I formation is resonant at 310 nm at the ground state equilibrium geometry. This $5500\,\mathrm{cm}^{-1}$ difference is still fairly close to the iodine spin–orbit splitting, and any surface crossings can reasonably be assumed to take place at shorter bond distances. The intensity ratio of the I/I* channels will then be determined by three effects: The Franck–Condon overlap with the ground state wave function(s), which favors the I channel; the possible decay of HgI_2 into I + Hg + I, which becomes energetically accessible at higher excess energies ($\lambda_1 < 355$ nm) and favors the I* channel; finally, the transition dipole matrix element, which probably favors the I* channel.[10(a)] The second contribution can be easily estimated from classical trajectory calculations, while the others require more detailed knowledge of the PES and wave functions. In general, we will assume the measured branching ratio of about 3.7:1 I:I* at $\lambda_1 = 310$ nm *ad hoc*. With these simplifications, the I and I* channels differ only by the excitation energy above the as-

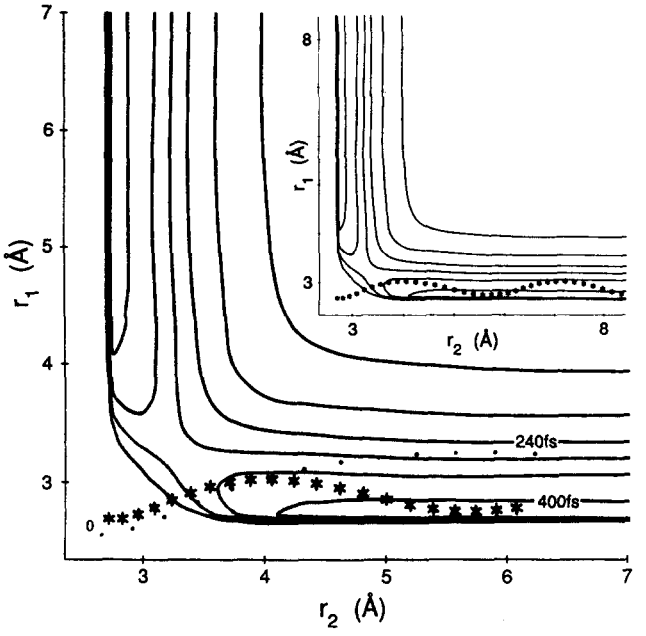

FIG. 13. Contour plot of the potential surface from Eq. (4). The tightness of the transition scale can be adjusted by varying β_1, which was found to be the most important parameter in reproducing the experimental results. The averaged trajectories for I* (*) and I (·) are shown; they originate at the turning point corresponding to the particular energy of excitation. Note that no oscillations are executed near the transition state, as the reaction time is comparable to the vibrational period of reactant and products, and that the I* channel corresponds to faster, smaller amplitude vibrations. The insert shows an expanded view where two full oscillations are shown.

ymptote, and the position of the classical turning point at which the wave packet originates.

We use the standard Hamiltonian

$$H=\frac{1}{\mathscr{M}}(p_1^2+p_2^2)+\frac{1}{\mathscr{M}_{12}}p_1p_2+V(r_1r_2), \qquad (6)$$

where the p_i are the momenta canonically conjugate to the HgI bond distances in the three-particle center of mass coordinate system, and the $\mathscr{M}$'s are the appropriate effective masses. The calculation was performed at excitation energies of 8950 (I) and1350 cm^{-1} (I*) relative to the HgI dissociation limit, by importance sampling a Gaussian distribution of starting points with a width determined by the excited state potential gradient, laser bandwidth, and approximate width of the ground state probability density. Momenta were chosen with random orientations but satisfying energy conservation. Integration of the equations of motion was carried out using Adam's predictor corrector method,[19] until the trajectories had become asymptotic ($r_i > 6$ Å). In view of the strong assumptions already made concerning the potential functions, this very simple treatment of the initial conditions is justified, particularly since the excitation energies used in the present study access only unbound states of the I–Hg–I system. This fact, combined with excitation of sufficient bandwidth, leads to the formation of initial superposition states localized near the inner turning point of the transition state. As a check of stability, several calculations were also carried out with a LEPS potential, different parameters in Eq. (4), and different choices of excess energy and width of the initial position distribution. The results were qualitatively the same, and we have chosen the above parametrization and set of assumptions because it yielded the best overall agreement with experiment.

The most important results of two hundred simulations for each channel are summarized in Table II. Averaged trajectories for the I and I* channels are shown in Fig. 13. They were obtained by summing trajectories going into the same final channel. The I channel, with its higher excess energy, moves to the products faster (<240 fs), and has a lower vibrational frequency (HgI anharmonicity) and larger vibrational amplitude. The I* channel moves more slowly (<400 fs reaction time), and has less internal energy, corresponding to more rapid, smaller amplitude vibrations. Since the two channels in this simple model differ only by their excitation energy and trajectory origins, this "equipartition" of higher available energy leading to higher internal and translational excitation is to be expected (within a single channel, higher vibrational energy of course entails lower translational energy, and *vice versa*).

In either case, the reaction time is sufficiently short that no oscillations are executed near the transition-state region. In the TS region, where probe absorption at 620 nm occurs, the I* channel wave packet lags the I channel by about 80 fs. The I channel also has a smaller acceptance angle for decay into I + HgI; 60% of the trajectories at 8950 cm^{-1} excess energy above the HgI dissociation limit actually dissociate into I + Hg + I; while full dissociation is also energetically allowed in the I* channel, almost none occurs. In the early time motion near the saddle point, product translation and vibration are strongly coupled as the normal coordinates are intermediate between symmetric/asymmetric stretching and HgI vibration/translation; this could account for the shifts in vibrational period observed for the first two peaks in Fig. 4(b), although it is also possible that the first peak has a large contribution from total dissociation.

The vibrational distributions of the HgI product in the two channels were found to be peaked at $v = 10$ in the I* channel and $v = 26$ in the I channel. Figure 14 shows typical distributions obtained from 100 nondissociative trajectories for each channel. None of the surfaces tried here produced bimodal distributions which could explain the observed results by a single channel model (other than Landau–Zener crossing).

2. HgI fluorescence spectra and the observed FTS transients

In order to compare the above results quantitatively with experiment, the HgI product fluorescence resulting at various probe times and frequencies from the two channels must be known. We will concentrate on the 390 nm probe experiment, since they correspond to separated HgI fragments, for which the spectroscopy is known. The potential parameters for the HgI X and B states in Table I represent an average of the best available literature values. The Morse

TABLE II. Trajectory calculations for the I and I* channel, using the PES in Fig. 13.

	I* channel	I channel
Excess energy[a]	1350 cm^{-1}	8950 cm^{-1}
Reaction time[b]	400 fs	240 fs
Full dissociation[c]	4%	60%
Average HgI v''[d]	13 ± 8	22 ± 8

[a] Energy above the I–Hg–I total dissociation limit distributed in the two collinear degrees of freedom.

[b] Here simply taken as the time required for trajectories to reach the asymptotic region of the PES at r larger than 7 Å; the temporal dependence of the position of the wave packet center is given in Fig. 13.

[c] To Hg + 2I or Hg + I + I*.

[d] Values are average (not peak) and standard deviation.

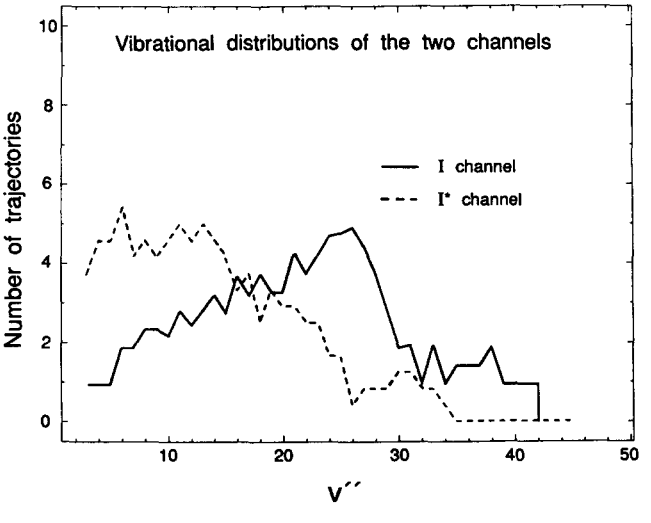

FIG. 14. HgI product vibrational distributions for the I channel (solid) and I* channel (dashed).

representations and transition dipole are sufficiently accurate such as not to introduce any noticeable spectral changes for a laser bandwidth in excess of 100 cm^{-1}.

The spectra are calculated by numerical integration of the vibrational Schrödinger equation in the following steps.[20] All X manifold bound states and vibrational wave functions are calculated. All B manifold states accessible by a 390 nm probe are calculated; in order to include emission into the continuum, at X manifold continuum wave functions accessible from the B manifold at several frequencies in the 420–460 nm range are evaluated. This results in a full set of Franck–Condon factors, which were found to be in good agreement with those previously reported.[9(b),10(b)] A lower state population distribution (Fig. 14) is assumed, and the distribution of B states from absorption of 390 nm radiation of the appropriate bandwidth is calculated. For each B state, the fractional parentage of X vibrational states is stored. The emission spectrum back to the ground electronic state is then evaluated, and for each transition, the original parent v'' distribution before pumping is known. The calculation was also performed with a $J = 100$ rotational term in the HgI potential function, and found to yield very similar results. Rotation was therefore again neglected, with the same understanding that the effective PES for the I–Hg–I system is rotationally averaged and cannot explain "slow" modulations of the data resulting from rotational anisotropy (see below). Finally, the experimental branching ratio of the I* and I channels was included to weight the individual contributions of the two channels to the overall fluorescence.

The results for the I* and I channels are shown in Figs. 15 and 16. The contributions of the two channels to the total fluorescence intensity are seen to be very different. The dashed band shows the spread of originally probed (v'') vibrational states as a function of frequency. The general trend is a slow decrease in v'' until continuum emission sets in at ~430 nm, where v'' rises again. For example, if one could somehow look at fluorescence of HgI formed in the I* channel only, detecting at 360 nm would reveal the dynamics of reactions yielding HgI at about $v'' = 22$, whereas detection at 428 nm would reveal the dynamics leading to $v'' = 5$ product. Fortunately, the two channels have widely varying contributions at different frequencies. The ratio of I/I* intensities is shown in Fig. 17, and in terms of it we can understand the 310/390 transients: where the ratio is larger than 1, the I channel dominates, where it is less than 1, the I* channel is more important. We now consider the various emission wavelengths of the 310/390 experiment in turn.

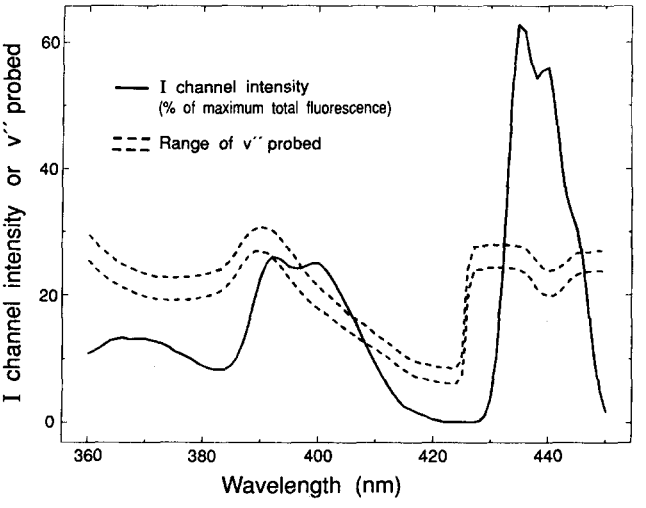

FIG. 16. Same as Fig. 15 for the I channel. The average vibrational energy of probed product HgI is much higher in this case.

At a detection wavelength of 360 nm, the I channel dominates. That transient probes highly excited ($v'' \sim 28$) molecules with a large internal and translational energy. The vibrational period at $v'' = 28$ is about 1 ps, as observed experimentally in the recurrences [Fig. 4(b)]. The very large first peak most likely also has a contribution from the I + Hg + I channel, which makes up 60% of the product

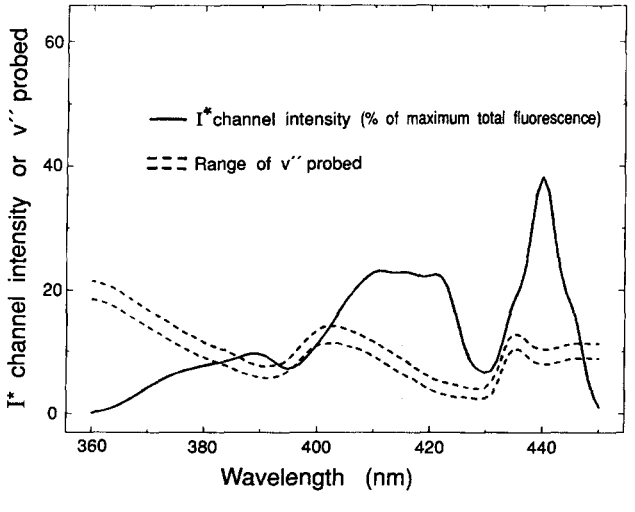

FIG. 15. Contribution on the I* channel to the total fluorescence spectrum, assuming a product vibrational distribution as calculated in the classical trajectory simulations; this includes the I/I* 3.7:1 observed branching ratio. The dashed lines bracket two standard deviations of the vibrational product distribution contributing to a given emission frequency.

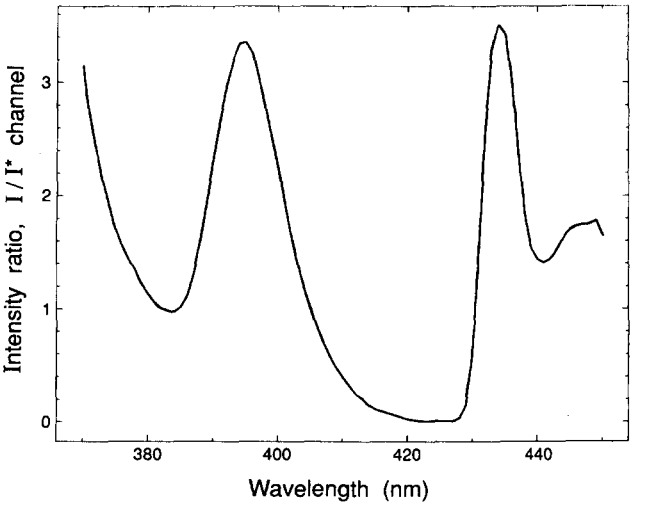

FIG. 17. The contributions of the two reaction channels to the product fluorescence vary as a function of frequency. The 360 and 432.5 nm fluorescence is seen to be due mainly to the I channel, whereas the 427.5 nm fluorescence is almost exclusively due to the I* channel; the 440 nm fluorescence contains contributions from both.

from the lower lying I surface (the I + Hg + I* channel is essentially closed at 310 nm, see Table II). At 427.5 nm, the I* channel is the most important contribution. As seen in the trajectory calculations, the product vibrational distribution is much lower. At 427.5 nm, the emission spectrum probes vibrational states around $v'' = 5 \pm 2$, in good agreement with the 300 fs oscillation period in Fig. 6. Resonance has not yet been completely achieved at the first peak, which is truncated. At 432.5 nm, the continuum emission becomes important, and the I channel is most important again. Hence, the transient again shows a large first peak (perhaps partly due to full dissociation) followed by recurrences corresponding to a distribution of HgI states around $v'' = 28$, as seen in Fig. 6. Finally, at 440 nm, the contribution of the channels is I*:I 40:60, close to the experimentally observed spectrum, which shows rapid oscillations corresponding to lower vibrational excitation in the I* channel, and a larger first peak corresponding to the I channel [Fig. 4(a)]. To a good approximation then, the transients at various frequencies can be constructed by averaging together pure I (large first peak, ~1 ps recurrences) and I* (oscillations near 300 fs) transients with weights and vibrational frequencies appropriate for the detection frequency.

The ratio in Fig. 17 is qualitatively very similar to the difference spectrum in Fig. 5. At 360 and 432.5 nm, the difference is a large positive fraction of the total signal; the first peak in the FTS transient is being probed, which contains more I channel signal, corresponding to a ratio above unity in Fig. 17. At 427.5 nm, the difference becomes a sizeable negative fraction of the total signal: The second peak, mostly due to the I* channel, contributes more, and the ratio in Fig. 17 is correspondingly small. Finally, at 440 nm, the difference is small compared to the total signal: I and I* contribute equally, and the ratio in Fig. 17 is near unity. It should be noted, however, that in the region between 400 and 420 nm, the difference spectrum predicts the I and I* channels to contribute equally, while the ratio in Fig. 17 indicates a progressive change from an I to an I* type transient. The region near 395 nm, where the difference is dramatic, is not easily accessible experimentally. Furthermore, the width and height of the local maximum near 395 nm in Fig. 17 is fairly sensitive to the choice of vibrational distribution, and could lead to a refinement of the potential function with a more complete theoretical treatment.

Dispersed fluorescence probing is thus a very powerful tool in understanding the FTS behavior. Looking at certain well-defined frequencies allows one to probe a specific reaction channel, and even specific vibrational levels in the reaction channel. Although the lack of information on the PES does not allow such a quantitative comparison for the 310/620 experiments, which probe the reaction closer to the transition state, a few salient features emerge by comparing the transients with the classical trajectory calculations and fluorescence simulations. Referring to Fig. 13, the difference in average translational energies can account for a 100 fs lag of the I* channel wave packet with respect to the I channel wave packet at 4–5 Å into the dissociation. Based on this, one would expect two peaks in the FTS transients, the first one about 80 fs from time zero (I), the second another 100 fs later (I*). This corresponds closely to the observations presented in Sec. III B. The actual peak separation is twice as wide; this may reflect a shift in the transition frequency for the probe beam, since the trajectories do not follow the same path, and the excited state PES leading to B HgI in the I and I* channels need not be identical in shape.

To summarize, the classical trajectory calculations combined with a quantum mechanical evaluation of the HgI emission spectra, are in good agreement with many of the observed features of the FTS spectroscopy. The two stretching coordinates are the most important on the time scale of the bond breaking, and the two-dimensional model looks like a promising basis for a more extensive treatment of the problem including bending modes and fragment rotation. A full quantum calculation will be reported in a separate publication.[21]

V. CONCLUSIONS

In this paper, we have presented an FTS study of the HgI_2 reaction:

$$IHgI^* \rightarrow [IHgI]^{\ddagger *}_{Q_v Q_{v'} q} \rightarrow HgI + I.$$

The molecular motions on the femtosecond time scale of the dissociation process, which involve two predominant degrees of freedom, were time resolved. Their fingerprint was found in the oscillatory behavior of the transients, which open a direct experimental window on the transition state, as the symmetric and antisymmetric stretching modes of the parent HgI_2 are converted to the translational and single vibrational degree of freedom of the HgI + I products.

Several experimental parameters were varied to study the details of the reaction: The choice of probe wavelength allowed a probing of the dissociating wave packet on early and late time scales. The fluorescence spectrum of HgI, pumped at 390 nm, revealed a richness of detail, with different spectral regions resulting from different channels of the dissociation reaction. This yielded dramatically different vibrational oscillatory patterns in transients at different wavelengths, due to the different vibrational and translational energy distributions in the I and I* channels.

We have also studied, and reported previously,[8(b)] the polarization anisotropy of the spectra, an example of which is shown in Fig. 18.[22] This way both the "scalar" and "vector" properties of the reaction were obtained. From the data presented in this paper we found a dissociation time of ~300 fs, and different vibrational periods (~300 fs and 1 ps) for the nascent HgI product along the two (I and I*) channels. From the data in Fig. 18 we obtained a coherence time of ~1 ps and deduced the angular momentum of the fragment $J_{max} \sim 80$.

The intuitive simplicity of the FTS transients has been put on a more quantitative foundation by comparison with classical trajectory calculations of the dissociation reaction and quantum calculations of the HgI fragment spectroscopy. Even the simplest two surface model, neglecting any possible crossings, yields a wealth of information on the vibrational and translational product distributions, which can be

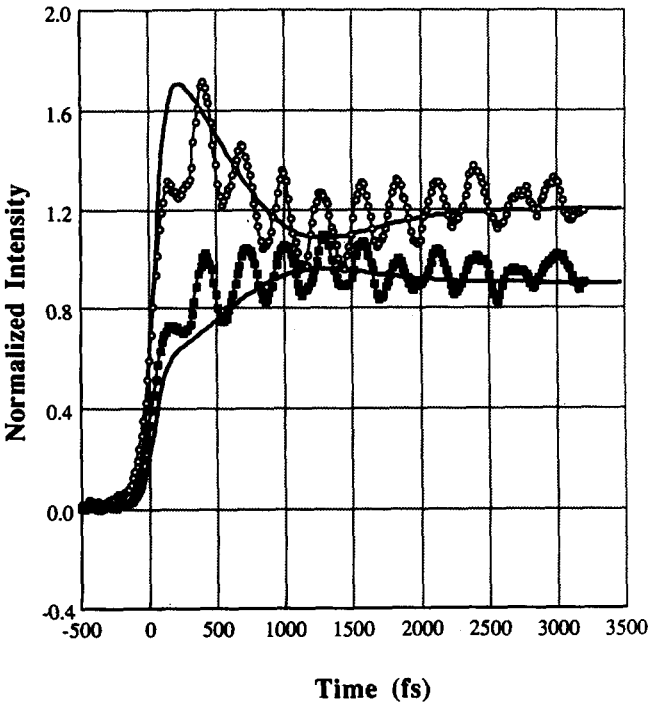

FIG. 18. FTS transients taken from $\lambda_1 = 310$ nm and $\lambda_2 = 390$ nm and detection at $\lambda_{det} = 427.5$ nm. The data is shown after normalization of the asymptotes to 1.2 and 0.9 for parallel (open circles) and perpendicular (filled squares) transients, respectively. The theoretical curves were generated using formulas derived in Ref. 8(b). The important feature to note is the complementary change of the transients when the polarization is changed; the oscillatory behavior is, however, unchanged. (See also Fig. 6.)

made to agree well with experimental observations by an appropriate choice of the PES. The quantum simulation of HgI fluorescence resulting from product molecules with well-defined vibrational distributions is as rich with structure as the observed transients.

FTS of dispersed molecular fluorescence, together with polarization methods, now make it possible to study these elementary reactions with multidimensional PES's. The femtosecond dynamics in such systems reflects the nature of the transition state and the different trajectories leading to products. It is therefore natural to extend these studies to a number of similar reactions in an attempt to map out the surface dynamics.

ACKNOWLEDGMENT

This work was supported by a grant from the Air Force Office of Scientific Research.

[1] A. H. Zewail, Science **242**, 1645 (1988); and referenced therein.
[2] A. H. Zewail and R. B. Bernstein, Chem. Eng. News **66**, 24 (1988).
[3] M. J. Rosker, M. Dantus, and A. H. Zewail, J. Chem. Phys. **89**, 6113 (1988).
[4] M. Dantus, M. J. Rosker, and A. H. Zewail, J. Chem. Phys. **89**, 6128 (1988), and references cited therein.
[5] R. B. Bernstein and A. H. Zewail, J. Chem. Phys. **90**, 829 (1989).
[6] T. S. Rose, M. J. Rosker, and A. H. Zewail, J. Chem. Phys. **91**, 7415 (1989).
[7] T. S. Rose, M. J. Rosker, and A. H. Zewail, J.Chem. Phys. **88**, 6672 (1988); M. J. Rosker, T. S. Rose, and A. H. Zewail, Chem. Phys. Lett. **146**, 175 (1988).
[8] (a) R. M. Bowman, M. Dantus, and A. H. Zewail, Chem. Phys. Lett. **156**, 131 (1989); (b) M. Dantus, R. M. Bowman, J. S. Baskin, and A. H. Zewail, *ibid.* **159**, 406 (1989).
[9] (a) J. Maya, J. Chem. Phys. **67**, 4976 (1977); IEEE J. Quantum Electron. **QE-15** 579 (1979); (b) K. Wieland, Helv. Phys.Acta **2**, 46 (1929); **14**, 420 (1941); K. Wieland, Z. Elektrochem. **64**, 761 (1960); K. S. Viswanathan and J. Tellinghuisen, J. Mol. Spectrosc. **98**, 185 (1983); (c) F. M. Zhang, D. Oba, and D. W. Setser, J. Phys. Chem. **91**, 1099 (1987).
[10] (a) H. Hofmann and S. R. Leone, J. Chem. Phys. **69**, 3819 (1987); (b) J. A. McGarvey, Jr., N. H. Cheung, A. C. Erlandson, and T. A. Cool, *ibid.* **74**, 5133 (1981); N. H. Cheung and T. A. Cool, J. Quant. Spectrosc. Radiat. Transfer **21**, 397 (1979).
[11] For reviews see R. Bersohn, J. Phys. Chem. **88**, 5145 (1984); J. P. Simons, *ibid.* **88**, 1287 (1984); and references therein.
[12] T. M. Mayer, B. E. Wilcomb, and R. B. Bernstein, J. Chem. Phys. **67**, 3507 (1977); T. M. Mayer, J. T. Muckerman, B. E. Wilcomb, and R. B. Bernstein, *ibid.* **67**, 3522 (1977); R. B. Bernstein, *Chemical Dynamics via Molecular Beam and Laser Techniques* (Oxford University, New York, 1982), p. 31; B. E. Wilcomb, T. M. Mayer, R. B. Bernstein, and R. W. Bickes, Jr., J. Am. Chem. Soc. **98**, 4676 (1976).
[13] R. L. Fork, B. I. Greene, and C. V. Shank, Appl. Phys. Lett. **38**, 671 (1981).
[14] R. L. Fork, C. V. Shank, and R. T. Yen, Appl. Phys. Lett. **41**, 223 (1982).
[15] A. H. Zewail, J. Chem. Soc. Faraday Trans. 2, **85**, 1221 (1989).
[16] JANAF Thermochemical Tables, Natl. Stand. Ref. Data Ser. Natl. Bur. Stand. 37, 2nd ed. (1971).
[17] W. R. Wadt, J. Chem. Phys. **72**, 2469 (1980).
[18] R. D. Levine and R. B. Bernstein, *Molecular Reaction Dynamics and Chemical Reactivity* (Oxford University, Oxford, 1987).
[19] W. H. Press, B. P. Flannery, S. A. Teukolsky, and W. T. Vetterling, *Numerical Recipes* (Cambridge University, Cambridge, 1986).
[20] B. R. Johnson, J. Chem. Phys. **67**, 4086 (1977).
[21] M. Gruebele and A. H. Zewail (in preparation); preliminary results of the full quantum calculations accurately reproduce the FTS transients and the vibrational distributions obtained by classical trajectory calculations..
[22] Similar polarization effects were observed when the probe wavelength was tuned off resonance to 620 nm, where the probing occurred solely in the transition-state region. We observe changes in the relative intensities of the I and I* channels with polarization. We shall use this in future studies to distinguish the different torques in the I and I* channels.